machines

MDPI

Article

The Influence of Suspension Elastokinematics on Vehicle Handling and Stability

Albert Basiul, Vidas Žuraulis, Robertas Pečeliūnas and Saugirdas Pukalskas *

Department of Automobile Engineering, Faculty of Transport Engineering, Vilnius Gediminas Technical University, Plytinės Str. 27A, 10105 Vilnius, Lithuania; albert.basiul@linqo.eu (A.B.); vidas.zuraulis@vilniustech.lt (V.Ž.); robertas.peceliunas@vilniustech.lt (R.P.)
* Correspondence: saugirdas.pukalskas@vilniustech.lt; Tel.: +370-655-29-573

Abstract

This study investigates the influence of suspension elastokinematics on vehicle handling and stability through a combined research of experimental testing and numerical simulation. Laboratory tests were conducted on the front suspension of a Mercedes-Benz S320 using a quarter-car test rig equipped with specialized sensors to measure wheel displacements, steering angles, camber, and accelerations. Complementary dynamic tests were carried out under real driving conditions, including braking in a turn and "fishhook" maneuvers, to capture suspension behavior under critical operating scenarios. Based on the experimental data, an MSC Adams/Car multibody simulation model was used, incorporating varying stiffness values of suspension elastomeric elements that replicated progressive aging and degradation effects. The simulation results were compared with experimental data to validate the model's predictive capability. Key findings indicate that reductions in elastomer stiffness significantly affect wheel kinematics, vehicle yaw response, and lateral acceleration, particularly during high-intensity maneuvers. The results underline the critical importance of accounting for elastomeric component degradation in suspension modeling to ensure vehicle safety and performance over the operational lifespan. The developed methodology demonstrates the effectiveness of integrating experimental measurements with advanced simulation tools to assess elastokinematic effects on vehicle dynamics.

Keywords: suspension; vehicle stability; elastokinematics; multibody simulation; MSC Adams/Car

check for updates

Academic Editors: Buyun Zhang and Chin-An Tan

Received: 1 October 2025
Revised: 9 November 2025
Accepted: 10 November 2025
Published: 12 November 2025

Citation: Basiul, A.; Žuraulis, V.; Pečeliūnas, R.; Pukalskas, S. The Influence of Suspension Elastokinematics on Vehicle Handling and Stability. *Machines* **2025**, *13*, 1047. https://doi.org/10.3390/machines13111047

Copyright: © 2025 by the authors. Licensee MDPI, Basel, Switzerland. This article is an open access article distributed under the terms and conditions of the Creative Commons Attribution (CC BY) license (https://creativecommons.org/licenses/by/4.0/).

1. Introduction

The elastokinematic behavior of modern automotive suspension systems is critically influenced by the compliance characteristics of elastomeric components, such as rubber bushings and mounts [1,2]. These elements facilitate controlled deformations under dynamic loads, contributing to vehicle handling and ride comfort. However, over time, elastomeric materials are subject to aging processes, including thermo-oxidative degradation, ozone exposure, and mechanical fatigue, leading to alterations in their mechanical properties [3–9]. Such degradation typically results in increased stiffness or softening, microcracking, and changes in damping characteristics, which can adversely affect suspension performance [10–12]. Notably, the aging of rubber bushings can cause deviations in wheel alignment parameters, such as toe and camber angles, under variable load conditions, thereby impacting vehicle stability and tire wear [13]. To address these issues, researchers have developed predictive models for the fatigue estimation of rubber bushings using

finite element analysis and virtual road load spectra [14]. Additionally, optimization techniques have been employed to adjust bushing compliance properties, aiming to enhance suspension durability and maintain desired elastokinematic characteristics throughout the vehicle's exploitation [15]. These studies underscore the importance of considering elastomer aging effects in the design and maintenance of suspension systems to ensure consistent vehicle performance and safety.

The long-term degradation of elastic suspension components, particularly rubber bushings, results in notable changes to their mechanical properties, thereby inducing measurable deviations in suspension kinematics. These deviations are typically expressed through alterations in suspension geometry under load, such as changes in wheel camber and toe angles, increased lateral and longitudinal compliance, and diminished steering accuracy. These phenomena have a detrimental effect on overall vehicle dynamics, including handling and stability performance, ride comfort, and tire wear uniformity. Due to their gradual and often imperceptible progression, such changes may remain undetected until they begin to impair driving stability or safety, which complicates diagnostic efforts and routine maintenance procedures. To address these challenges, several studies have introduced methods for predicting or compensating for the effects of elastomer aging. For instance, Brancati et al. [16] examined the use of magnetorheological bushings capable of adjusting their stiffness characteristics in real time according to varying operating conditions, thus counteracting the impact of material degradation. Similarly, Archut and Corves [17,18] proposed advanced multibody dynamic models that incorporate flexible body mechanics and inertial relief concepts in order to more accurately capture the evolving compliance behavior of suspension joints over time.

Some studies employ advanced rheological models and experiments to capture rubber bushing behavior under realistic conditions. For example, Zhao et al. [19] proposed a viscoelastic fractional Kelvin–Voigt model for a layered rubber damping element. They show that the fractional-order parameter allows "real-time characterization of the large-deformation response" of the material, fitting experimental stress–strain data more precisely than classical models. These constitutive models are sufficiently compact for real-time or hardware-in-the-loop simulation while capturing the rubber's complex viscoelastic dynamics.

On the material level, Shi et al. [20] performed comprehensive amplitude- and frequency-sweep tests on various rubber springs (bushings). They measured dynamic stiffness and the loss factor, revealing a pronounced amplitude dependence consistent with the Payne effect: as the strain amplitude increases, the loss factor initially rises, reaching a peak before progressively decreasing. These experimental studies confirm that automotive rubber bushings dissipate substantial energy through hysteresis, especially under large cyclic strains, and that this damping can be reliably quantified by dynamic tests.

Ce Liang et al. [21] emphasized the importance of continuous monitoring of elastomer degradation and the implementation of adaptive or active suspension systems to ensure driving safety, occupant comfort, and long-term dynamic performance throughout a vehicle's exploitation period.

Rubber bushing stiffness is notably nonlinear and varies with preload, as well as excitation amplitude and frequency. Schutte and Sextro incorporated measured rubber bushing data into a multibody axle model and emphasized that bushing stiffness depends on excitation frequency and amplitude [22]. They modeled the bushings using Kelvin–Voigt elements (spring in parallel with damper) because simple linear models cannot capture the frequency-dependent elasticity and damping. Likewise, Shi et al. reported that the storage modulus of rubber springs drops significantly as amplitude increases, reflecting the Payne effect, while the loss factor varies non-monotonically with strain and frequency [20]. These

findings demonstrate that rubber elasticity is not constant—it decreases with increasing deformation and varies over the suspension's operating frequency range.

Blundell, in his study [23], examined the influence of rubber bush compliance on vehicle suspension movement, emphasizing that even small elastic deformations in bushings can significantly affect suspension geometry—particularly toe and camber angles—under operational loads. By employing a multibody simulation approach, he proved that neglecting bushing compliance in modeling may lead to inaccurate predictions of suspension behavior. His findings highlight the critical importance of integrating realistic elastic properties of rubber components into elastokinematic analyses to ensure accurate vehicle handling performance.

Beyond the studies cited above, a growing body of work explicitly compares classic linear suspension models—such as linear quarter-car representations and Kelvin–Voigt bushing elements—with nonlinear and elastokinematic formulations. Adduci et al. review bushing modeling in multibody frameworks and show that linear spring–damper surrogates often miss amplitude- and frequency-dependent effects, leading to handling prediction errors when compliance is significant [24]. Likewise, Zhang et al. (2021) quantify how rubber-bushing stiffness and torsion-bar load alter double-wishbone suspension stiffness; an Adams-based multibody model aligned with nonlinear theory ($\leq$2.3% error), underscoring the need to move beyond linear assumptions [25]. Recent computational studies further benchmark nonlinear elastokinematic solvers against linearized or Simscape-type baselines, demonstrating that linear models systematically under-estimate toe/camber variations and compliance-driven geometry changes under load [26]. In dynamic response, Tran et al. (2024) report regimes where linear and nonlinear suspensions behave similarly at low speeds, but diverge markedly at higher speeds or broadband/random excitations—conditions under which nonlinear effects degrade ride indices if ignored [27]. Complementary comparisons of linear–flexible versus nonlinear multibody formulations likewise document measurable discrepancies in predicted handling when bushing nonlinearity and multi-axis coupling are neglected [28]. Previous studies have shown that the elastokinematic behavior of modern automotive suspensions is critically influenced by the compliance characteristics of elastomeric components, such as rubber bushings and mounts. These components, which facilitate controlled deformations under dynamic loads, are subject to aging processes (including thermo-oxidative degradation, ozone exposure, and mechanical fatigue) that alter their mechanical properties—resulting in variations in stiffness, microcracking, and changes in damping, all of which can adversely affect vehicle handling, ride comfort, and overall stability. In light of these findings, it has been decided to conduct this study with the aim of evaluating the impact of suspension elastokinematics on vehicle handling and stability. To achieve this, established literature methodologies will be employed to perform laboratory tests under various driving conditions, and the empirical results will be modeled using MSC Adams/Car 2013 (MSC Software Corporation, Irvine, CA, USA) simulation software [29].

A broad body of research shows that suspension stiffness and damping directly shape the propagation of road-induced vibrations through the vehicle structure and, consequently, interior NVH. Since their attachment points, which provide the intended movement, are an integral part of the suspension elements, bushing stiffness measurably alters vibration amplitudes and spectral content transmitted to the body, underscoring stiffness selection as a primary lever for both comfort and vibro-safety [30]. For sub-300 Hz road-noise/vibration, the suspension is a dominant transfer path; thus, even small layout changes can significantly influence interior acoustic and vibratory responses [31]. In viscoelastic rubber mounts/bushings, the stiffness–damping pair functions as a vibration isolator, and accurate parameter identification is essential to predict energy dissipation and transfer func-

tions from road to body [1]. Recent developments further demonstrate targeted tuning via frequency-dependent or adaptive components—e.g., SMA-based rubber composite dampers and hydraulic bushings—to reconcile the comfort–handling trade-off by tailoring effective stiffness and loss across operating conditions [2,32,33]. Within this context, the present study's elastokinematic analysis quantifies how compliance-induced geometry changes, together with realistic damping/stiffness, affect handling stability under transient maneuvers.

This study deliberately focuses on plant-side characterization and open-loop validation rather than controller synthesis. Specifically, we quantify how load-dependent elastokinematics and bushing-stiffness degradation affect handling-relevant responses (yaw rate, lateral acceleration, trajectory radius) by calibrating an MSC Adams/Car model against field and laboratory measurements. The resulting calibrated model is intended to serve as a control-ready plant, enabling future developments in online estimation and active/semi-active suspension strategies.

2. Materials and Methods

In investigating the influence of suspension elastokinematics on vehicle handling and stability, comprehensive experimental tests of both full-vehicle dynamics and suspension behavior were first conducted. To examine the suspension response under varying driving conditions, both field and laboratory tests were performed. Based on the experimental results, the magnitudes of suspension component deformations were calibrated within the MSC Adams/Car simulation environment. Using the modified vehicle model, additional simulations were carried out, enabling an accurate assessment of the impact of suspension elastokinematics on the vehicle's dynamic characteristics.

2.1. Experimental Tests

2.1.1. Laboratory Tests

Laboratory investigations were carried out using the sprung and unsprung masses of the front suspension of a Mercedes-Benz S 320 (W220). The suspension system was mounted on a structural test rig frame, allowing unrestricted movement, with suspension mounting points corresponding to the original suspension geometry of the Mercedes-Benz S 320 used in the study (Figure 1). Wheel rolling on the test rig was induced by a rubber belt driven by an electric motor through two chain-connected rotors [34]. When a load was applied to the wheel, the rubber belt remained undeformed due to the bearing assembly positioned beneath it.

The specifics of the quarter car test rig involved keeping suspension kinematics (together with elastokinematics) in its natural operation, which is influenced only by the excitation from wheel-pavement interaction. As body (sprung mass) oscillation motion (pitching and rolling) is limited by test rig construction, analysis of suspension elements motion in terms of stiffness–damping property change is more objective and predictable. The main purpose of this research part was to receive the information about the nature of wheel motion in three operation modes, as these motions were measured directly with the RV-4 sensor system. The achieved wheel's motion addresses the preliminary vehicle handling and stability issues, which will be analyzed in further research.

For the suspension elastokinematic measurements, a Kistler RV4 instrument (Figure 1) was employed and mounted on the front left wheel (Kistler Instrumente GmbH, Sindelfingen, Germany). Displacements were collected by processing the data from several angular sensors, achieving an accuracy of $\pm 0.2^{\circ}$ for wheel orientation and ± 0.5 mm for wheel position. All the data were collected using a Kistler DAS3 system (Kistler Instrumente GmbH, Sindelfingen, Germany) with a 200 Hz logging frequency. This system is designed

to measure five degrees of freedom of the wheel, representing the unsprung mass of the vehicle: vertical, longitudinal, and lateral displacements relative to the body, steering and camber angles, and angular rotation [35]. With these measurement functions, the system can be applied to wheelbase variation analysis, the design and optimization of suspension as a dynamic-kinematic system (springs and dampers), wheel geometry adjustment, and investigations of vehicle behavior under different driving conditions.

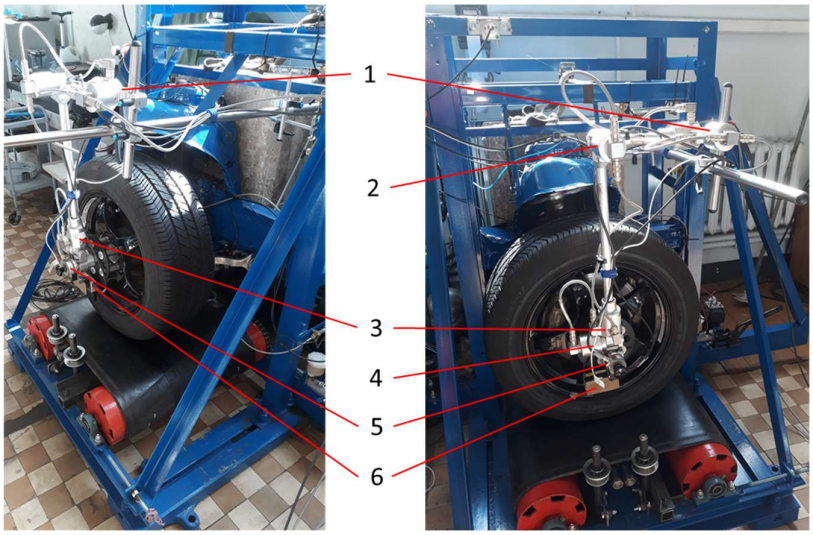


Figure 1. Test rig for the right front wheel of the Mercedes-Benz S 320 front axle with measurement equipment: 1 and 2—wheel longitudinal and vertical motion sensors; 3—wheel steering angle sensor; 4—wheel camber angle sensor; 5—wheel pulse transducer for angular speed; 6—wheel acceleration sensor.

The laboratory measurements were carried out under the following modes:

- Non-loaded (lifted) wheel kinematics measurement;
- Wheel braking with no steer angle at 20 km/h;
- Wheel braking with a steer angle at 20 km/h.

The purpose of measuring the rotations of the lifted wheel was to determine the kinematic parameters of the wheel and suspension during steering, since in the course of steering, the suspension components undergo displacements, causing a simultaneous shift of the wheel center, which influences the test results. In Section 3, a comparison will be made between the kinematic parameters (when the wheel is lifted and subjected to steering rotations) and the dynamic and elastokinematic parameters (when the wheel is loaded, rolling on the belt, steering, and braking).

2.1.2. Field Tests

Dynamic measurements of the vehicle suspension elastokinematics were carried out with a Mercedes-Benz S 320 (W220) (Figure 2) on a closed driving track with a dry asphalt surface. The same Kistler RV-4 wheel vector sensor was used for these tests with a triaxial accelerometer mounted on it. Its measuring range is $\pm$50 g with 80 mV/g sensitivity and frequency response up to 1 kHz. The combination of these types of sensor systems allowed for a detailed assessment of wheel movement and the influence of suspension elastokinematics.

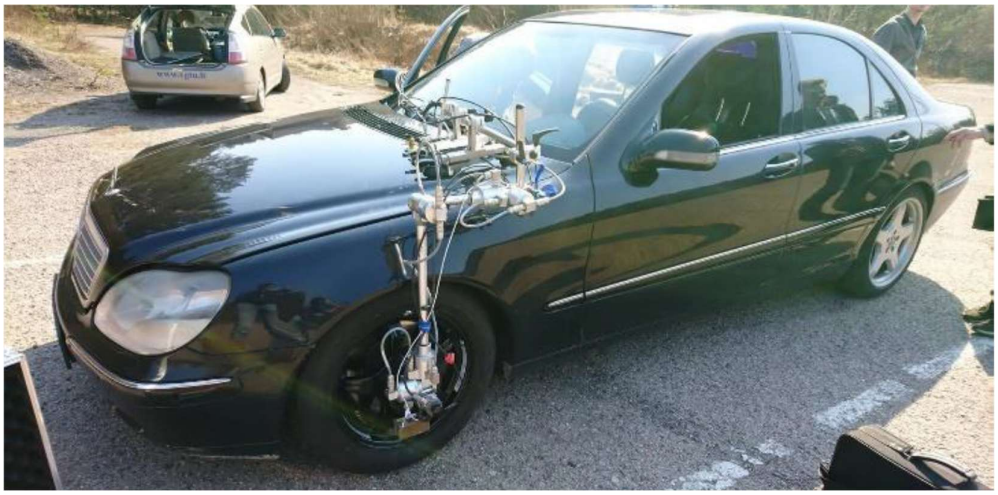


Figure 2. Mercedes-Benz S 320 vehicle and Kistler RV4 dynamic measurement equipment.

The suspension of the test vehicle was in proper technical condition, meeting all regulatory requirements. During the tests, the following maneuvers were performed:

- Acceleration up to 40/50/60 km/h followed by low-intensity braking (Mean Fully Developed Deceleration ~2.8 m/s^2);
- Acceleration up to 45/50 km/h and braking with right side cornering;
- Acceleration up to 45/50 km/h and braking with left side cornering.

Before the tests, the vehicle's static load was measured. The purpose of this stage was to determine the quarter-car mass corresponding to the left wheel, in order to apply the same parameters for static tests on a specialized quarter-car test rig [34]. For the mass measurements, the scales from Dini Argeo were used, ensuring an accuracy of ±0.4 kg, and the results showed that the load on the front left wheel suspension was equivalent to 447.8 kg.

2.2. Numerical Tests

The last part of the research was conducted in a simulation environment of MSC Adams Car using a validated vehicle model that is capable of showing the influence of suspension elastokinematics on vehicle handling and stability at higher driving speeds. This part of the experiment involved extended research conditions in a safe and reliable manner. For the simulations, a front-wheel-drive vehicle model with integrated tire, front and rear suspension, steering, braking, powertrain, and body sub-systems was chosen from the software library (Figure 3), with the following main parameters:

- Vehicle mass—1565 kg;
- Wheelbase—2720 mm;
- Track width—1552 mm;
- Powertrain layout: front engine, rear-wheel drive;
- Suspension types: (a) front—MacPherson (Figure 4a); (b) rear—multi-link (Figure 4b);
- Center of gravity position: x = 1600 mm; y = 762 mm; z = 700 mm;
- Vehicle body mass moments of inertia: I_x = 221 kg/m^2; I_y = 1070 kg/m^2; I_z = 1180 kg/m^2.

The iteration ratio of 0.001 was used for each simulation in order to keep high computational accuracy and the performance of the virtual vehicle model as close to real-world conditions as possible.

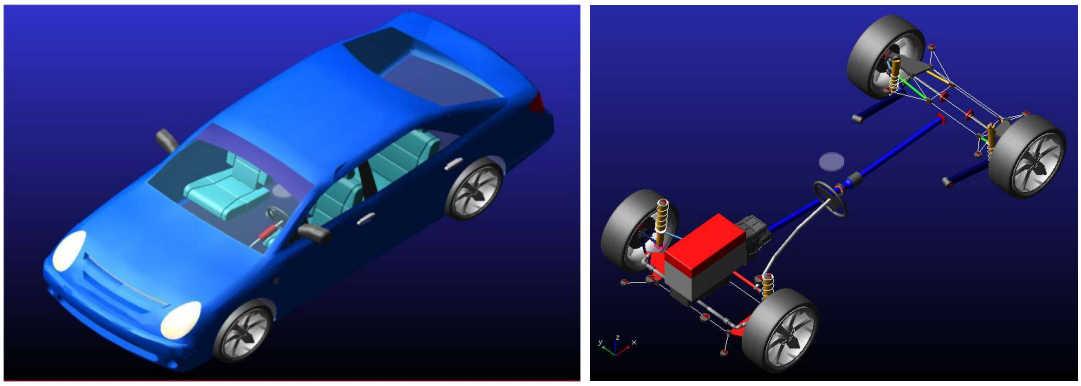
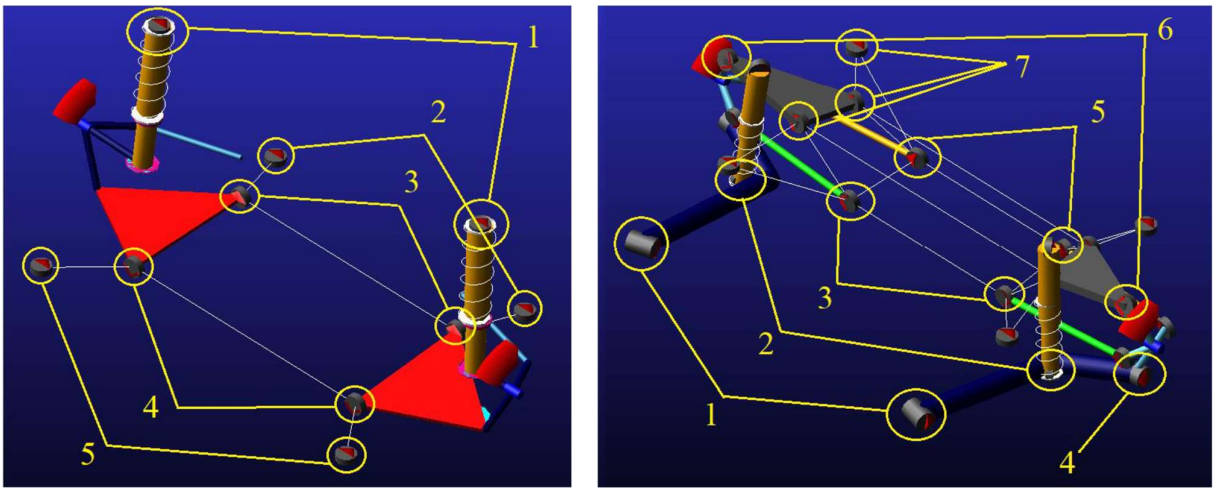


Figure 3. MSC Adams/Car software model of a front-wheel-drive vehicle.



(**a**) (**b**)

Figure 4. Elastomeric elements of the suspension layouts selected in MSC Adams/Car software: (**a**) front MacPherson suspension: 1—shock absorber mounts; 2—rear body-to-suspension rubber elements; 3—rear bushings of the lower control arm; 4—front bushings of the lower control arm; 5—front body-to-suspension rubber elements; (**b**) rear multi-link suspension: 1—bushings of the lower front arms; 2—shock absorber mounts; 3—bushings of the upper front arms; 4—bushings of the lower hub section; 5—bushings of the upper rear arms; 6—bushings of the upper hub fork; 7—body-to-suspension bushings.

Based on the results of dynamic and laboratory suspension tests, corrections were applied to the selected software model and simulation parameters in order to obtain similar wheel movement characteristics. Once comparable results were achieved in the simulations and validated against the dynamic and laboratory test data, the system parameters of the model were left unchanged, with adjustments in each simulation case applied only to the stiffness values of the front and rear suspension elastomeric components. After modifying the stiffness parameters of the suspension elastomeric elements, the vehicle was tested in simulations to determine changes in driving behavior. The vehicle model dynamics were analyzed through the following maneuver simulations:

- Braking in a turn;
- "Fishhook" maneuver.

For the MSC Adams/Car computer simulation of vehicle motion during braking along a cornering trajectory, the following main input data were used:

- Turning radius—150 m;
- Braking intensity rise time—0.6 s;

- Maximum braking time—4 s;
- Steering wheel fixed in position;
- Engaged gear—4th.

The purpose of the "fishhook" maneuver is to determine the vehicle's stability limit according to predefined steering inputs (open-loop maneuver type). The "fishhook" maneuver consists of two consecutive steering inputs in opposite directions (Figure 5). The MSC Adams/Car software allows the same simulations to be repeated multiple times with varying stiffness parameters of the suspension elastomeric components.

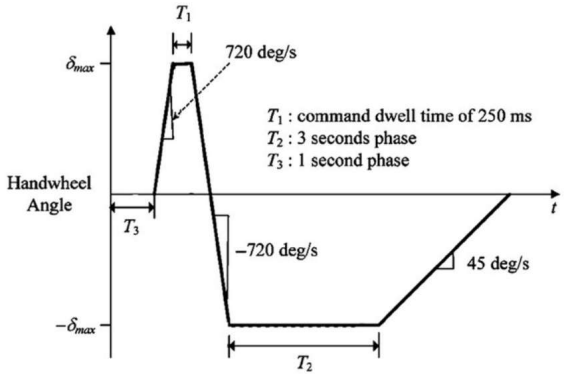


Figure 5. Steering angle in fishhook maneuver [36].

Main input parameters in the MSC Adams/Car software for performing the simulations were as follows:

- Initial vehicle speed—105 km/h;
- Engaged gear—4th.

For the first turn to the right, the following parameters were applied:

- Steering wheel angular velocity for the first turn: 520°/s;
- Transition time from straight-line driving to the first turn—0.1 s;
- Duration of the first turn maneuver—0.4 s.

For the second turn to the left, the following parameters were applied:

- Steering wheel angular velocity for the second turn: 760°/s;
- Transition time from the first right turn to the second left turn—0.2 s;
- Duration of the second turn maneuver—0.8 s.

3. Results

3.1. Results of Laboratory Tests

In the initial tests with the lifted wheel, wheel kinematics were investigated (Figure 6), i.e., the displacements of the wheel axis depending on the steering angle and direction. At the maximum steering angle of 9.19° to the right, the wheel was displaced along the longitudinal axis, in the rolling direction, by 1.9 mm. At the same steering angle, along the transverse axis, the wheel was displaced toward the vehicle center by 3.87 mm (Figure 6b). When the wheel was steered to the opposite side at an angle of 14.6°, the longitudinal displacement occurred against the rolling direction by 1.77 mm (Figure 6a), while along the transverse axis, the wheel was displaced away from the vehicle center by 3.42 mm (Figure 6b). Wheel displacement accelerations were not evaluated in these tests.

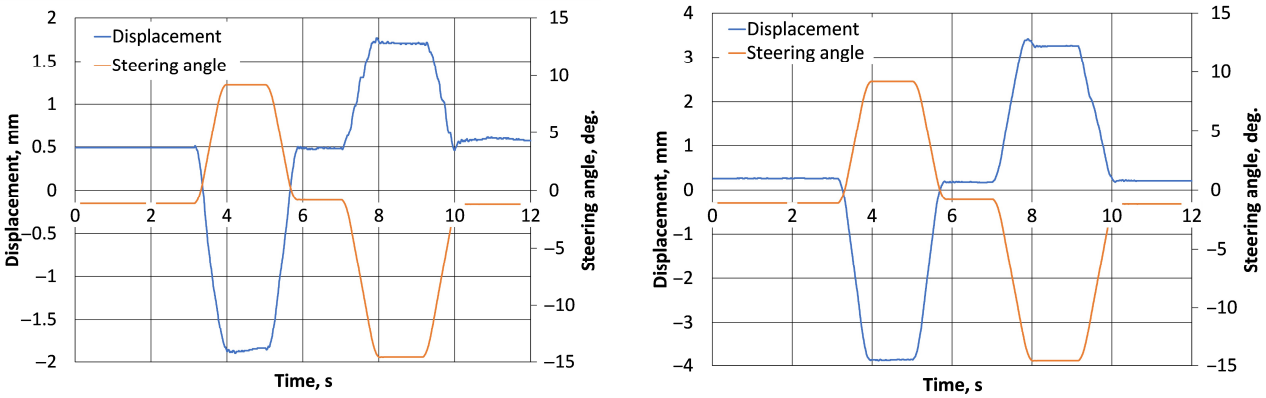


Figure 6. Displacements of the lifted wheel during steering: (**a**) along the longitudinal axis; (**b**) along the transverse axis.

When the quarter-car test rig simulated a speed of 20 km/h, the wheel was steered twice to the left and once to the right during rolling. Under straight-line driving conditions, the wheel displacement curve (Figure 7a) exhibits the same characteristics as in straight-line driving with braking (at 20 km/h), with an average displacement of 0.5 mm. The average wheel displacement (when steered to the left, between 12 and 15 s of the test (Figure 7a), reached up to approximately 1.6 mm. Since the wheel is subjected to rolling resistance, the longitudinal displacement in dynamic tests, occurring opposite to the rolling direction, is smaller compared to the kinematic tests in which the lifted wheel's kinematic characteristics were investigated. During the right turn (17–21 s of the test), the wheel was displaced longitudinally in the rolling direction, reaching up to 3.8 mm. Considering the lateral displacements, the curves show that when the wheel was steered to the left (Figure 7b), the lateral displacement varied around 2.5 mm (12–15 s of the test) away from the vehicle's center of mass. When the wheel was steered to the right, the lateral displacement reached up to 1.5 mm (17–21 s of the test) toward the vehicle's center of mass.

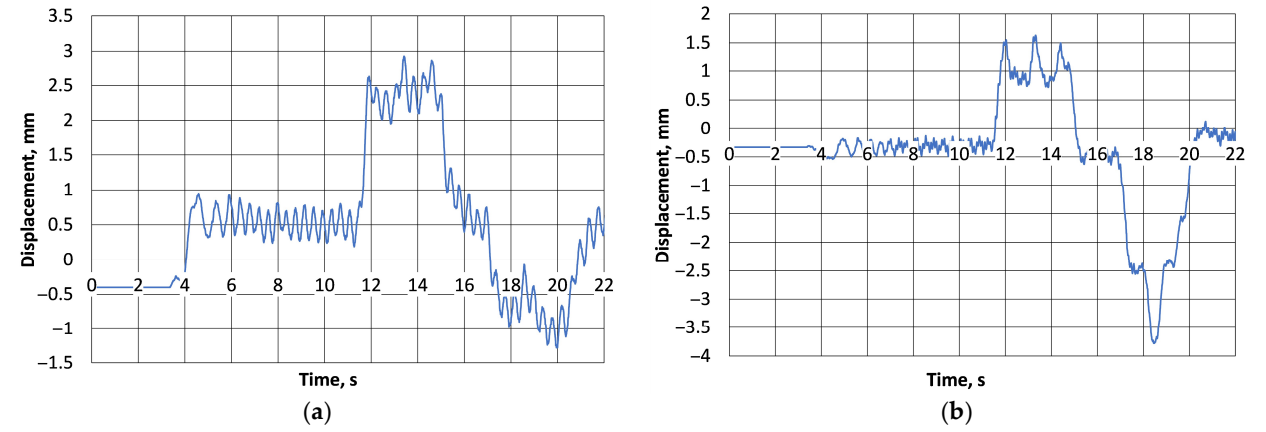
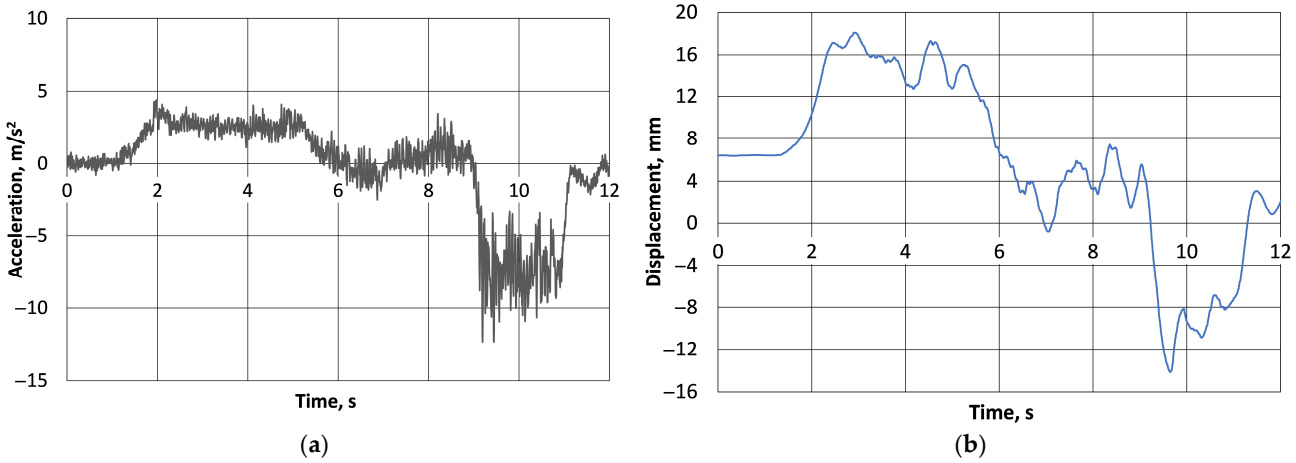


Figure 7. Wheel displacement characteristics during steering at a speed of 20 km/h: (**a**) longitudinal displacement characteristics; (**b**) lateral displacement characteristics.

3.2. Results of Field Tests

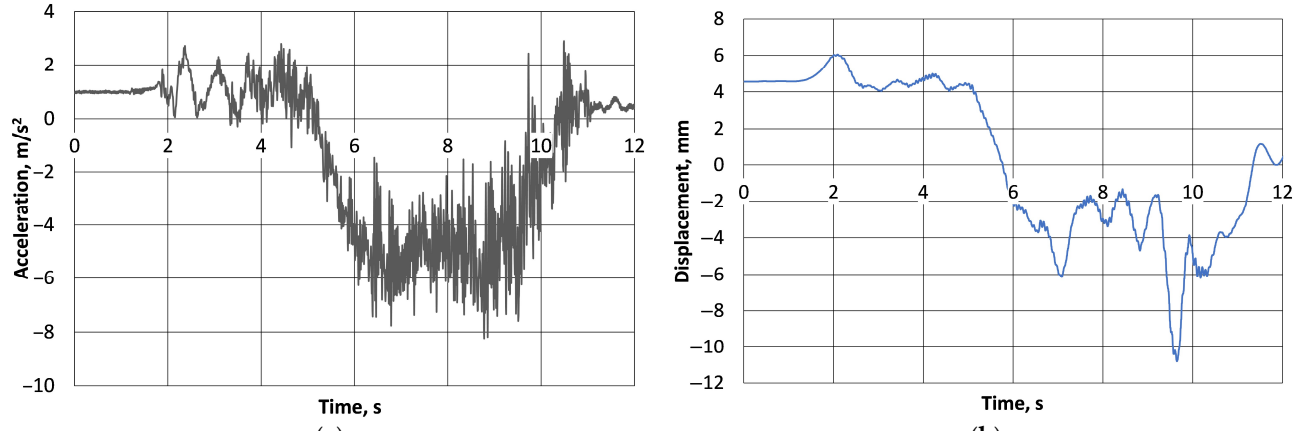
During tests of acceleration and braking to the right (at 50 km/h), it can be observed that braking begins at the 9th second (Figure 8, braking phase). The longitudinal displacements (Figure 8b) and lateral accelerations (Figure 9a) indicate that between 5 and 9 s (before braking begins), the vehicle starts moving to the right (following a curved trajectory). As the vehicle moves to the right, the left wheel shifts inward relative to the

vehicle body, i.e., it is displaced rearward along the longitudinal axis and inward along the transverse axis. At the onset of braking, the following can be observed: (a) the maximum longitudinal wheel acceleration (Figure 8a) varies around 8 m/s^2, while the displacement (Figure 8b) from the start of the curved trajectory to the onset of intense braking is 28 mm; (b) the lateral wheel acceleration (Figure 9a) during intense braking varies around 6 m/s^2, while the displacement (Figure 9b) from the start of the curved trajectory to the onset of intense braking is 14 mm. When intense braking begins, after the parameter spike (at 9 s), the suspension quickly returns to its initial state (after the 10th second); this change can be explained by the tire losing grip with the road surface (wheel slip begins). Since the lateral acceleration (Figure 9a) and displacement (Figure 9b) vary, and under intense braking the parameter reaches its maximum and then decreases (with the suspension returning to its initial state), while the steering angle remains constant (and in places increases), it can be assumed that the left wheel is slipping.



(**a**) (**b**)

Figure 8. Characteristics of the left wheel of the Mercedes-Benz S 320 during a right turn at an acceleration speed of 50 km/h: (**a**) longitudinal accelerations of the left wheel; (**b**) longitudinal displacements of the left wheel.



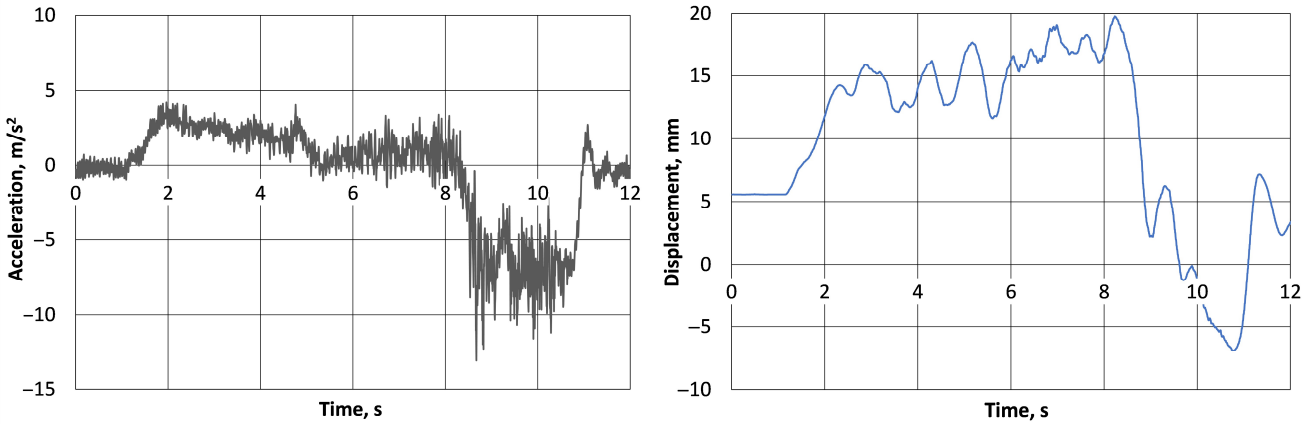
(**a**) (**b**)

Figure 9. Characteristics of the left wheel of the Mercedes-Benz S 320 during a right turn at an acceleration speed of 50 km/h: (**a**) lateral accelerations of the left wheel; (**b**) lateral displacements of the left wheel.

During the tests of acceleration and braking to the right (at 45 km/h), it can be observed that (a) the maximum longitudinal wheel acceleration under intense braking is 9 m/s^2, while the displacement (from the start of the curved trajectory to the onset

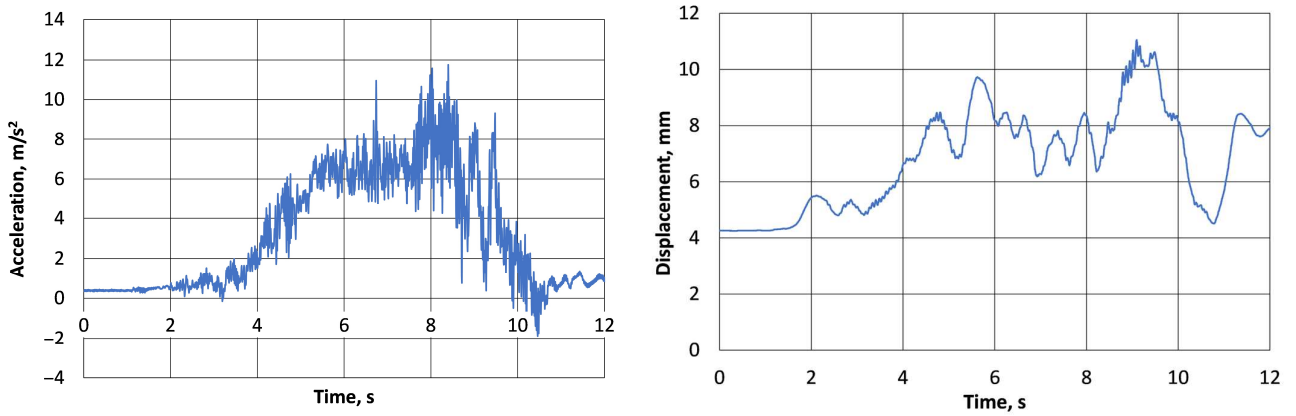
of intense braking) is 23.5 mm; (b) the lateral wheel acceleration under intense braking is 7 m/s^2, while the displacement (from the start of the curved trajectory to the onset of intense braking) is 12 mm.

During the tests of acceleration and braking to the left (at 50 km/h), it can be observed that braking begins at the 8th second, and after it ends, the suspension returns to its initial state (Figure 10). The longitudinal displacements and accelerations (Figure 10) and the lateral accelerations (Figure 11a) show that in the 4–8 s interval (prior to braking), the vehicle starts moving to the left (following a curved trajectory). As the vehicle moves to the left, the left wheel shifts outward relative to the vehicle body, i.e., rearward along the longitudinal axis and outward along the transverse axis. Between the 9th and 11th seconds, intense braking occurs. The maximum longitudinal wheel acceleration (Figure 10a) during intense braking reaches 8–9 m/s^2, while the displacement (Figure 10b) from the start of the curved trajectory to the onset of intense braking is 27 mm. The maximum lateral wheel acceleration (Figure 11a) reaches 8–9 m/s^2, while the displacement (Figure 11b) from the start of the curved trajectory to the onset of intense braking is 6.5 mm.



(**a**) (**b**)

Figure 10. Characteristics of the left wheel of the Mercedes-Benz S 320 during a left turn at an acceleration speed of 50 km/h: (**a**) longitudinal accelerations of the left wheel; (**b**) longitudinal displacements of the left wheel.



(**a**) (**b**)

Figure 11. Characteristics of the left wheel of the Mercedes-Benz S 320 during a left turn at an acceleration speed of 50 km/h: (**a**) lateral accelerations of the left wheel; (**b**) lateral displacements of the left wheel.

Comparing the left- and right-turn cases, it can be observed that the longitudinal displacements are similar, whereas the lateral displacements differ by about a factor of two.

This can be explained by the fact that along the longitudinal axis, the degree of freedom is the same in both cases, while for lateral displacements, when the wheel moves outward, the suspension stiffness is greater (the degree of freedom of the left wheel during a left turn is smaller).

During the tests of acceleration and braking to the left (at 45 km/h), it can be observed that (a) the maximum longitudinal wheel acceleration under intense braking is 10 m/s^2, while the displacement (from the start of the curved trajectory to the onset of intense braking) is 24 mm; (b) the lateral wheel acceleration under intense braking is 9.5 m/s^2, while the displacement (from the start of the curved trajectory to the onset of intense braking) is 6.5 mm. The results demonstrate that the parameter distribution is similar at both 45 and 50 km/h.

The comparison between both experimental approaches revealed that the wheel displacement deviation between the bench test and the full-vehicle experimental data did not exceed 4.3% during straight-line braking and 15.6% during braking-in-cornering. These results confirm that the bench test data accurately represent the suspension's elastic–kinematic characteristics and can be reliably used for vehicle-level dynamic analysis.

3.3. Elastokinematic Modeling Using MSC Adams/Car Software

Based on the results of the laboratory tests, analogous simulations of intensive braking were performed. At a speed of 20 km/h under straight-line braking conditions, the wheel displacement was 3.8 mm in the laboratory tests, while in the simulations it was 3.97 mm (a difference of 4.3%). Furthermore, with minimal error, it was possible to replicate the simulation of braking along a cornering trajectory using the results of dynamic tests. For example, at a speed of 50 km/h in the dynamic tests, the wheel displacement under intensive braking was 27 mm, whereas in the simulations, the displacement value at the same moment was 32 mm (a difference of 15.6%). The larger discrepancy between the dynamic and simulation results (during the braking-in-cornering maneuver) can be explained by the fact that in the simulations, the vehicle wheels lock, while in the dynamic tests, the probability of wheel slip was reduced by the Anti-lock Braking system (ABS).

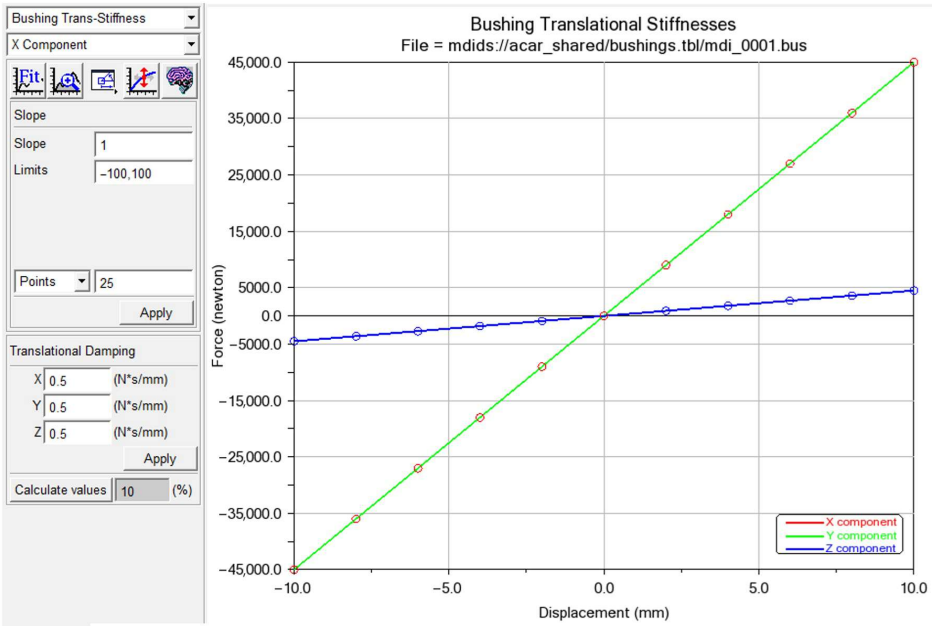
For the simulations, the baseline stiffness values of the suspension elastomeric components were selected as provided by the MSC Adams/Car software. The stiffness of the elastomeric elements is defined by the relationship between the applied force and the displacement of the element along a given axis. In each simulation stage, this parameter relationship was considered linear. In general, the multibody model assigns stiffness values to each bushing element according to three components (Figure 12a), the most sensitive of which is in the Y direction; therefore, this research investigates the effect of this component in particular. In order to evaluate the nonlinearity of the model elements, a damping of 0.5 N·s/m was applied to the bushings. For the front axle MacPherson suspension (Figure 4a), the standard stiffness parameters of the elastomeric elements provided by MSC Adams/Car were reduced by factors of 3 and 6 in order to determine the vehicle behavior under varying suspension elastokinematic properties. For the rear axle multi-link suspension (Figure 4b), the stiffness parameters of the elastomeric elements (comparative parameters) were reduced by a factor of 2 relative to the standard values.

Each suspension elastomeric element has its own defined parameter characteristic; therefore, in the first stage of simulations, tests were carried out using the standard (initial) stiffness parameters of the suspension bushings. In general, the stiffness characteristics of all elements can be grouped into two categories:

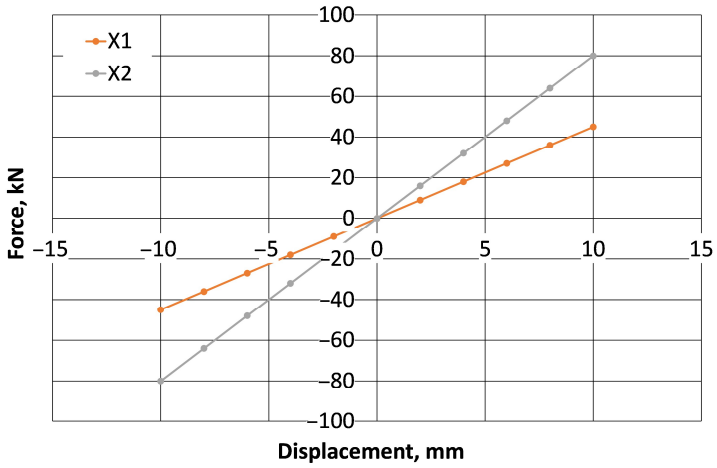
1. Standard stiffness parameter dependency of elastomeric elements ranging from −45 kN to 45 kN for displacements between −10 mm and 10 mm;

2. Standard stiffness parameter dependency of elastomeric elements provided by the MSC Adams/Car software, ranging from −80 kN to 80 kN for displacements between −10 mm and 10 mm (Figure 12). This group included the following elastomeric elements:

- Upper elastomeric mounts of the front MacPherson suspension shock absorbers;
- All body-to-suspension connection points of the front MacPherson suspension.



(**a**)



(**b**)

Figure 12. Initial stiffness characteristics of elastomeric elements in MSC Adams/Car software: (**a**) stiffness components and damping values; (**b**) selected stiffness characteristics of the first group of elastomeric elements (X1) and of the second group of elastomeric elements (X2).

All other elastomeric elements of the front and rear suspension were assigned to the first group. According to the axial parameter distribution, the characteristics remained the same. In subsequent simulations, the stiffness characteristics of the elastomeric elements were reduced relative to the initial parameters suggested by MSC Adams/Car.

In the second stage of simulations, the stiffness characteristics of the elastomeric elements were reduced relative to the initial values: by a factor of 3 for the front suspension and by a factor of 2 for the rear suspension (Figure 13a).

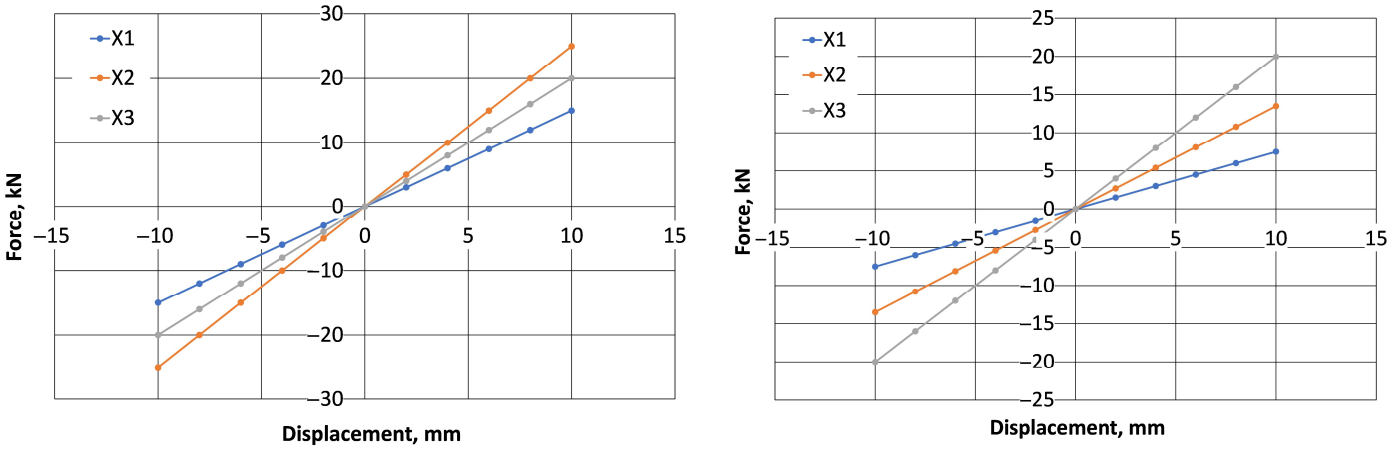


Figure 13. Elastomeric stiffness characteristics in the second (**a**) and third (**b**) simulation stages in MSC Adams/Car: stiffness characteristics of the first group of front MacPherson suspension elastomeric elements (X1); stiffness characteristics of the second group of front MacPherson suspension elastomeric elements (X2); stiffness characteristics of the rear multi-link suspension elastomeric elements (X3).

In the third stage of simulations, the stiffness characteristics of the elastomeric elements were reduced relative to the initial values: by a factor of 6 for the front suspension and by a factor of 2 for the rear suspension (Figure 13b).

The results of each simulation were analyzed according to the following parameters:

- Vehicle yaw rate;
- Vehicle longitudinal and lateral acceleration;
- Wheel side slip angles.

The road surface was specially generated in the Adams subprogram Road Builder and was used in all simulations to represent the conditions of real dry asphalt pavement. For comparisons of suspension and wheel kinematic results, the kinematic parameters of the front bushing of the left lower control arm of the front MacPherson suspension were selected (Figure 14). Since the primary objective of investigating wheel kinematic parameters is to determine their direct influence on vehicle handling and stability, it was assumed that the linear kinematic parameters of the joint connecting the lower control arm of the front MacPherson suspension to the hub directly characterize the wheel behavior in the simulations, i.e., the kinematic parameters of the lower control arm joint were considered equivalent to the wheel kinematic parameters. As the MSC Adams/Car software does not apply measurements at the center of the joint axis in simulations, it was assumed that the wheel kinematic parameters would be derived from the indicators of the front bushing of the left lower control arm of the front MacPherson suspension, using trigonometric equations. The present study was intentionally structured as a multi-stage validation framework, combining bench tests, field tests, and simulation analysis. Each stage served a distinct purpose: the bench tests focused on quantifying the suspension's elastic characteristics under controlled laboratory conditions; the field tests evaluated the actual compliance and natural dynamics of the suspension system in real driving conditions; and the simulation stage integrated both experimental datasets to generalize the results and predict vehicle-level dynamic behavior. Therefore, these experimental levels were designed not to replicate identical test conditions, but to complement each other and progressively expand the research context.

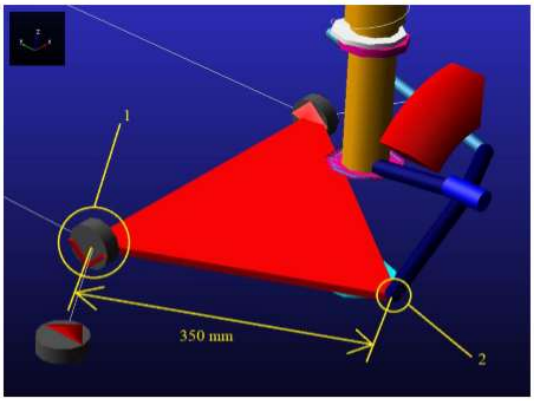


Figure 14. Diagram of the left lower control arm of the front-wheel-drive vehicle model in MSC Adams/Car software: 1—front bushing of the left lower control arm of the front MacPherson suspension; 2—ball joint of the left lower control arm of the front MacPherson suspension.

3.3.1. Braking in a Turn: MSC Adams/Car Computer Simulation Results

To compare the results of the vehicle simulations, additional braking tests in turn maneuvers were performed. In the MSC Adams/Car simulation, braking begins in the first second of the test, when a significant displacement jump is recorded in the front bushings of the left lower control arm of the MacPherson suspension (Figure 15a). Comparing the first and second simulation stages, it can be observed that in the second stage, the displacements increased by 49%, and in the third stage by 77%. Calculations using trigonometric equations showed that the instantaneous wheel displacements at the onset of braking (with the initial suspension stiffness values) were 10.4 mm; after the second simulation stage, the displacement increased to 14.7 mm (an increase of 29%), and after the third simulation stage to 16.5 mm (an increase of 37%).

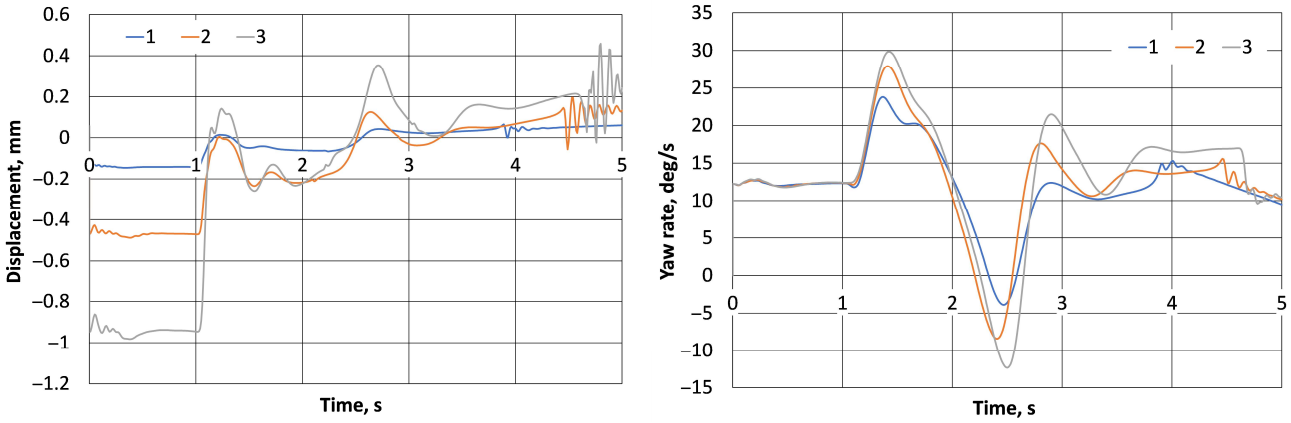


Figure 15. Results of braking in a turn maneuver simulations in MSC Adams/Car: 1—first-stage simulation with standard suspension elastomeric stiffness values; 2—second-stage simulation with reduced elastomeric stiffness (front suspension reduced by a factor of 3, rear suspension reduced by a factor of 2); 3—third-stage simulation with reduced elastomeric stiffness (front suspension reduced by a factor of 6, rear suspension reduced by a factor of 2): (**a**) displacements of the front bushing of the left lower control arm of the front MacPherson suspension; (**b**) yaw rates.

When braking in a corner, due to the locked steering wheel, vehicle controllability is lost throughout the entire braking path. This phenomenon is characterized by the curves of vehicle yaw rates (Figure 15b) and the trajectory radius parameters of the vehicle's motion (Figure 16a). The graphical outputs of the simulations showed that during braking

in a corner (with a cornering radius of 150 m), the vehicle with the initial elastomeric stiffness values had only its front end outside the designated trajectory, while in the second and third simulation stages, the vehicle had entirely deviated from the intended path. The graphical results of the simulations demonstrate that the stiffness parameters of the elastomeric elements have a direct influence on vehicle controllability when the steering wheel is locked.

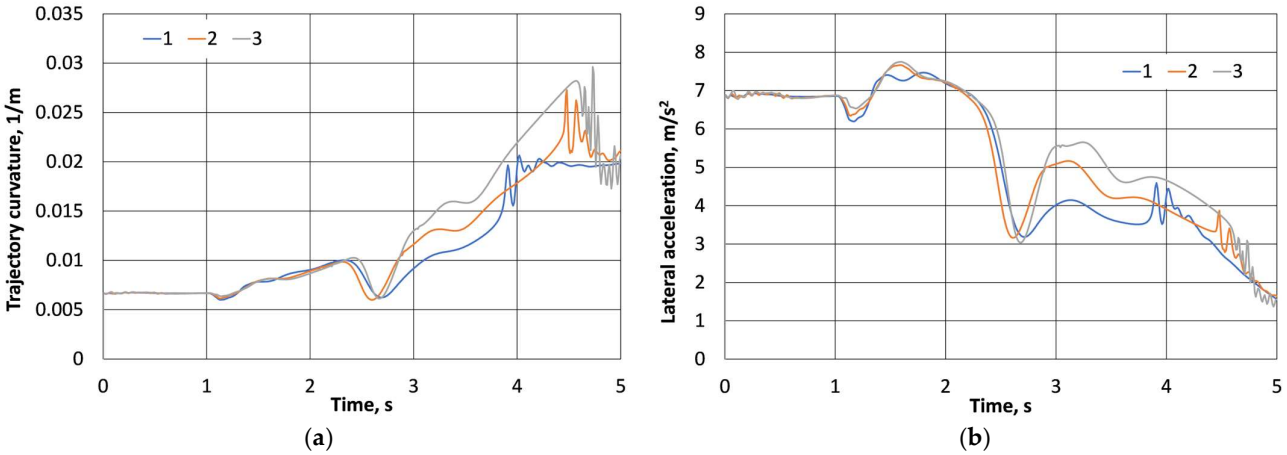


Figure 16. Results of braking in a turn maneuver simulations in MSC Adams/Car: 1—first-stage simulation with standard suspension elastomeric stiffness values; 2—second-stage simulation with reduced elastomeric stiffness (front suspension reduced by a factor of 3, rear suspension reduced by a factor of 2); 3—third-stage simulation with reduced elastomeric stiffness (front suspension reduced by a factor of 6, rear suspension reduced by a factor of 2): (**a**) vehicle trajectory radius; (**b**) vehicle lateral acceleration.

In terms of the vehicle yaw rate during each simulation (Figure 15b), in the second simulation stage, the yaw rate increased by 12% compared to the initial values, and in the third stage by 23%. This indicates that during braking, the vehicle in the second and third simulation stages performed rotations about the vertical axis more rapidly and at larger angles, which led to vehicle instabilities on the road.

The instabilities of the vehicle trajectory are demonstrated by the variations in the trajectory radii (Figure 16a). At the beginning of each simulation, the vehicle followed the predefined road trajectory. Once braking began, the vehicle exhibited understeer, with the largest values occurring for the vehicle with the initial elastomeric stiffness parameters. This phenomenon can be explained by the fact that with a stiffer suspension, the acting forces and the redistribution of the center of mass make it more difficult for the rear part of the vehicle to move outward from the corner center (i.e., to oversteer). After the braking increase phase ended, the vehicle in all simulation cases temporarily exhibited oversteer (with the trajectory directed toward the corner center), and the curve values were similar at this stage. Due to the locked wheels during braking and the fixed steering angle, the action of inertial forces caused the vehicle trajectory to change in the opposite direction. At approximately 2.5 s, the vehicle again began to understeer, though it still remained on the road. As braking continued, the final braking phase occurred, during which the vehicle developed oversteer. The results in Figure 16a show that in the second simulation stage, the vehicle trajectory radius decreased by 14% compared to the first stage over the interval of 2.5–4 s, and by 25% in the third stage. This indicates that in the final braking phase, as the suspension elastomeric stiffness decreases, the vehicle trajectory radius is reduced, leading to vehicle oversteer. Due to this increased turning tendency, in the second and third simulation stages, the vehicle deviated outside the designated trajectory boundaries.

In the final braking phase, the vehicle's lateral accelerations also changed (Figure 16b). The graphical results show that lateral acceleration increased as the suspension elastomeric stiffness decreased. Comparing the first and second simulations, the acceleration increased by 19% in the second stage and by 25% in the third stage.

3.3.2. Results of the "Fishhook" Maneuver Simulations in MSC Adams/Car

The results of the "fishhook" maneuver showed that in the first simulation stage, the displacements in the bushings of the front section of the lower control arm of the front MacPherson suspension were the smallest (Figure 17a). In the second simulation stage (with stiffness parameters reduced by a factor of 3 in the front MacPherson suspension and by a factor of 2 in the rear multi-link suspension), the displacements increased by 71.4%, while in the third stage (with stiffness parameters reduced by a factor of 6 in the front MacPherson suspension and by a factor of 2 in the rear multi-link suspension), they increased by 87.5%.

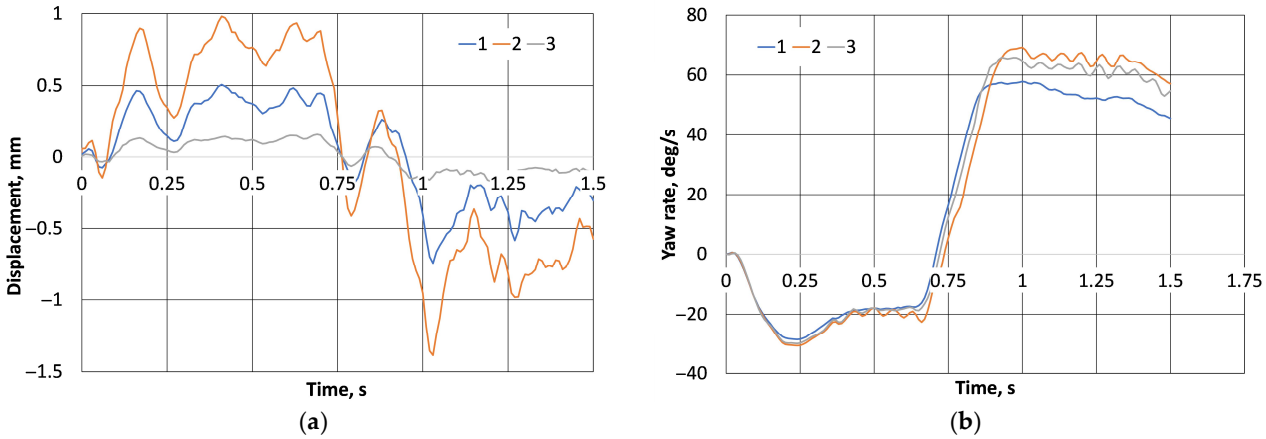


Figure 17. Results of the "fishhook" maneuver simulations in MSC Adams/Car: 1—first-stage simulation with standard suspension elastomeric stiffness values; 2—second-stage simulation with reduced elastomeric stiffness (front suspension reduced by a factor of 3, rear suspension reduced by a factor of 2); 3—third-stage simulation with reduced elastomeric stiffness (front suspension reduced by a factor of 6, rear suspension reduced by a factor of 2): (**a**) displacements of the front bushing of the left lower control arm of the front MacPherson suspension; (**b**) vehicle yaw rate.

Evaluating the linear and angular wheel displacements during critical vehicle maneuvering moments, it was observed that the left wheel displacements (calculated from the trigonometric formula) increased equally in the second and third stages by 51% when the vehicle turned right, and by 34% when the vehicle turned left. The vehicle yaw rate curves during right-hand turns were similar across all simulations (Figure 17b), indicating that in right turns, the vehicle followed the same trajectory in each simulation stage.

After the transition phase between turns, the vehicle executed a sharp left-hand turn. In each simulation stage, the vehicle performed the left turn differently. Comparing the first and second simulation stages, it can be seen that in the second stage, the vehicle executed the left turn more quickly and with a larger angle, corresponding to oversteer. The yaw rate in the second simulation stage increased by 25.4%.

During the third simulation, the vehicle executed the left turn with a lower yaw rate (the yaw rate in the third simulation stage increased by 19.4% compared to the first-stage simulation result) than in the second-stage simulations (Figure 17b), despite the fact that the front MacPherson suspension in the third stage had lower elastomeric stiffness parameters than in the second stage. This phenomenon can be explained by the highest variation of the vehicle's lateral acceleration (Figure 18). Lateral acceleration is determined by the

contact forces of the wheels, which are significantly affected not only by interaction with the road but also by the work of the suspension elements due to elastokinetics. The graphs show that in the second simulation stage, under critical vehicle maneuvers, the frequency of acceleration intensity was higher than in the third stage. The graphical results of the simulations indicate that the reduction in elastomeric stiffness in the front MacPherson suspension acts as a compensatory force during critical vehicle maneuvers, since part of the centrifugal force is absorbed by the oscillations of the front wheels.

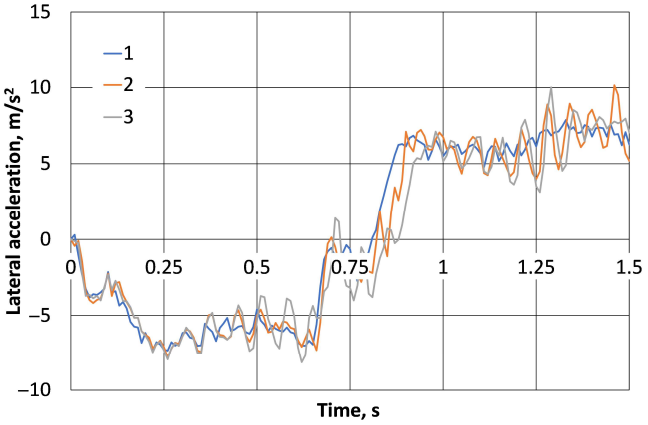


Figure 18. Vehicle lateral acceleration results of the "fishhook" maneuver simulations in MSC Adams/Car: 1—first-stage simulation with standard suspension elastomeric stiffness values; 2—second-stage simulation with reduced elastomeric stiffness (front suspension reduced by a factor of 3, rear suspension reduced by a factor of 2); 3—third-stage simulation with reduced elastomeric stiffness (front suspension reduced by a factor of 6, rear suspension reduced by a factor of 2).

4. Conclusions

The conducted research demonstrated that suspension elastokinematics and kinematics play an important role in determining vehicle handling, stability, and overall safety. Experimental investigations carried out on the Mercedes-Benz S320 front suspension, both in laboratory conditions and during real driving tests, provided valuable insight into the behavior of elastomeric elements under different loading and maneuvering conditions. The integration of these experimental results with numerical simulations in MSC Adams/Car using three different stiffness values of suspension elastomeric elements allowed for precise evaluation in more complicated driving conditions, like higher speeds, intensive braking, and cornering. The analysis of bench tests, multibody dynamic simulations, and experimental measurements of the entire vehicle revealed several consistent patterns in suspension behavior. The influence of bushing stiffness on vehicle dynamics was particularly evident: increasing the radial stiffness of the bushings by 20% reduced the lateral displacement of the wheel by approximately 7.8% and improved the smoothness of the vehicle's trajectory when braking in a turn by approximately 5.2%.

The study confirmed that the degradation of elastomeric components, simulated by progressively reducing stiffness values, has a significant impact on vehicle dynamics. Specifically, reduced stiffness leads to increased wheel displacements, higher yaw rates, and elevated lateral accelerations, particularly during critical maneuvers such as braking in a turn and the "fishhook" test. These effects translate into greater oversteer tendencies, reduced trajectory radii, and heightened risks of vehicle instability. Correlation analysis showed that elastically related wheel geometry parameters (wheel camber and toe) and vertical load changes directly affect steering precision and handling. It was observed that larger displacements from bushings can increase the vehicle's tendency to oversteer by up to 8% when lateral acceleration is high.

The results emphasize the necessity of incorporating realistic elastokinematic characteristics into suspension modeling and design processes. Accounting for elastomeric component wear and variability is essential to ensure reliable prediction of vehicle dynamics across the entire operational lifespan. Furthermore, the methodology presented—combining experimental testing with advanced multibody simulations—proved effective in quantifying elastokinematic influences and can be applied to the optimization of suspension systems in future vehicle development.

Author Contributions: Conceptualization, A.B. and V.Ž.; methodology, V.Ž. and R.P.; software, A.B. and V.Ž.; validation, A.B., V.Ž. and S.P.; formal analysis, V.Ž. and R.P.; investigation, A.B., V.Ž., R.P. and S.P.; resources, R.P. and S.P.; data curation, V.Ž.; writing—original draft preparation, A.B. and V.Ž.; writing—review and editing, R.P. and S.P.; visualization, V.Ž. and S.P.; supervision, V.Ž.; project administration, V.Ž. All authors have read and agreed to the published version of the manuscript.

Funding: This research received no external funding.

Data Availability Statement: Data are available upon request.

Conflicts of Interest: The authors declare no conflicts of interest.

References

1. Puma-Araujo, S.D.; Galluzzi, R.; Sánchez-Sánchez, X.; Ramirez-Mendoza, R.A. Study of Viscoelastic Rubber Mounts on Vehicle Suspensions with In-Wheel Electric Motors. *Materials* **2021**, *14*, 3356. [CrossRef] [PubMed]
2. Huang, Y.; Fan, Q.; Zhang, H.; Shao, L.; Shi, Y. Optimization of Dynamic Characteristics of Rubber-Based SMA Composite Dampers Using Multi-Body Dynamics and Response Surface Methodology. *Appl. Sci.* **2024**, *14*, 10063. [CrossRef]
3. Investigating the Service Life of Aged Elastomer Components. Available online: https://www.lbf.fraunhofer.de/en/projects/investigating-elastomer-service-life.html (accessed on 3 May 2025).
4. Cho, H.C.; Lee, S.H.; Cho, H.C.; Lee, S.H. *Study on the Long-Term Aging-Resistance of Anti-Vibration Rubber in the Vehicle*; SAE International: Warrendale, PA, USA, 2002.
5. Wu, J.; Luo, H.; Li, H.; Su, B.; Wang, Y.; Li, Z. The Influence of Hydrothermal Aging on the Dynamic Friction Model of Rubber Seals. *Polymers* **2020**, *12*, 102. [CrossRef] [PubMed]
6. Gaitanidou, A.; Tränkner, M.; Iosifidis, G.; DeSantis, R.; Efstathiadis, T.; Kalfas, A. Degradation of Elastomer Damping Component for High-Speed Bearings. *Eng. Proc.* **2025**, *90*, 54.
7. Bakar, M.; Sola-Wdowska, M.; Przybyłek, M.; Białkowska, A.; Zarzyka, I.; Hanulikova, B.; Masař, M. Investigation of Combined Aging and Mullins Stress Softening of Rubber Nanocomposites. *Polymers* **2024**, *16*, 3141. [CrossRef]
8. Yunzhou, F.; Honglei, Z. High-Temperature Fatigue Life Prediction Method for Rubber Bushing of New-Energy Vehicles Based on Modified Fatigue Damage Theory. *Mater. Res. Express* **2020**, *7*, 015346. [CrossRef]
9. Saha, T.; Bhowmick, A.K. Thermal and Thermo-Oxidative Degradation of Rubbers: Some Recent Studies. In *Degradation of Elastomers in Practice, Experiments and Modeling*; Heinrich, G., Kipscholl, R., Stoček, R., Eds.; Advances in Polymer Science; Springer International Publishing: Cham, Switzerland, 2021; Volume 289, pp. 209–238, ISBN 978-3-031-15163-7.
10. Sung, D.-U.; Busfield, J.; Ryu, Y.H. *Degradation of Vehicle Noise and Vibration by Ageing of Elastomers*; SAE International: Warrendale, PA, USA, 2017; p. 2017-01-0392.
11. Zehsaz, M.; Vakili-Tahami, F.; Paykani, A. Investigation on the Effects of Stiffness and Damping Coefficients of the Suspension System of a Vehicle on the Ride and Handling Performance. *Sci. Bull.* **2014**, *76*, 55–70.
12. Giese, U.; Kautz, S.; Schwarzendahl, C.; Thust, S. Mechanistic and Kinetic Studies on Degradation Processes of Rubber Types. In *Degradation of Elastomers in Practice, Experiments and Modeling*; Heinrich, G., Kipscholl, R., Stoček, R., Eds.; Springer International Publishing: Cham, Switzerland, 2023; pp. 317–344, ISBN 978-3-031-15164-4.
13. Duan, X.; Shangguan, W.-B.; Li, M.; Rakheja, S. Measurement and Modelling of the Fatigue Life of Rubber Mounts for an Automotive Powertrain at High Temperatures. *Proc. Inst. Mech. Eng. Part D J. Automob. Eng.* **2016**, *230*, 942–954. [CrossRef]
14. Knapczyk, J.; Maniowski, M. Elastokinematic Modeling and Study of Five-Rod Suspension with Subframe. *Mech. Mach. Theory* **2006**, *41*, 1031–1047. [CrossRef]
15. Kang, B.J.; Kim, N.W.; Kim, J.H.; Lee, Y.H.; Sin, H.-C. Improving the Durability of Automobile Suspension Systems by Optimizing the Elastomeric Bushing Compliance. *Proc. Inst. Mech. Eng. Part D J. Automob. Eng.* **2008**, *222*, 469–484. [CrossRef]
16. Brancati, R.; Di Massa, G.; Rocca, E.; Rossi, C.; Savino, S.; Timpone, F. Elasto-Kinematic Characteristics of Car Suspensions with Magneto-Rheological Bushings. In *Advances in Service and Industrial Robotics*; Ferraresi, C., Quaglia, G., Eds.; Mechanisms and Machine Science; Springer International Publishing: Cham, Switzerland, 2018; Volume 49, pp. 414–423, ISBN 978-3-319-61275-1.

17. Archut, J.-L.; Corves, B. Real-Time Multibody Simulation of Vehicle Wheel Suspensions of Different Topologies with Elastokinematic Properties. *Multibody Syst. Dyn.* **2025**, *63*, 255–271. [CrossRef]
18. Archut, J.-L.; Corves, B. Real-Time Flexible Multibody Simulation of a Vehicle Wheel Suspension with Elastokinematic Properties Based on Inertia Relief Modes. In *New Trends in Mechanism and Machine Science*; Rosati, G., Gasparetto, A., Ceccarelli, M., Eds.; Mechanisms and Machine Science; Springer Nature Switzerland: Cham, Switzerland, 2024; Volume 165, pp. 349–357, ISBN 978-3-031-67294-1.
19. Zhao, Z.; Meng, W.; Yan, B.; Liang, H.; Geng, Y.; Sun, Z. Study on the Dynamic Characteristics of Low-Frequency High-Stiffness Viscoelastic Damping Structures. *Materials* **2025**, *18*, 1446. [CrossRef] [PubMed]
20. Shi, Y.; Li, J.; Wang, Y.; Li, X.; Gao, Y.; Zhao, D.; Shi, B.; Zou, L.; Song, X.; Shang, Y. A Full Range Experimental Study of Amplitude- and Frequency-Dependent Characteristics of Rubber Springs. *Polymers* **2022**, *14*, 4662. [CrossRef] [PubMed]
21. Liang, C.; Li, M.; Li, Y.; Liang, J.; Han, Q. Friction Characteristics Analysis of Rubber Bushing with a Bionic Flexible Contact Surface Based on the Convex Hull Structure. *Polymers* **2023**, *15*, 606. [CrossRef]
22. Schütte, J.; Sextro, W. Tire Wear Reduction Based on an Extended Multibody Rear Axle Model. *Vehicles* **2021**, *3*, 233–256. [CrossRef]
23. Blundell, M.V. The Influence of Rubber Bush Compliance on Vehicle Suspension Movement. *Mater. Des.* **1998**, *19*, 29–37. [CrossRef]
24. Adduci, R.; Vermaut, M.; Perrelli, M.; Cosco, F.; Vanpaemel, S.; Naets, F.; Mundo, D. A Review of Bushing Modelling Approaches for MultiBody Simulations. *Mech. Mach. Theory* **2024**, *191*, 105496. [CrossRef]
25. Zhang, B.; Li, Z. Mathematical Modeling and Nonlinear Analysis of Stiffness of Double Wishbone Independent Suspension. *J. Mech. Sci. Technol.* **2021**, *35*, 5351–5357. [CrossRef]
26. Magri, P.; Gadola, M.; Chindamo, D.; Sandrini, G. A Comprehensive Method for Computing Non-Linear Elastokinematic Properties of Passenger Car Suspension Systems: Double Wishbone Case Study. *J. Comput. Nonlinear Dyn.* **2024**, *19*, 101006. [CrossRef]
27. Tran, H.N.; Pham, N.D. Analysis of a Bus Vertical Dynamic Performances—A Comparison between Linear and Nonlinear Suspension Systems. *J. Vibroeng.* **2024**, *26*, 1118–1132. [CrossRef]
28. Gao, J.; Han, P. Collaborative Optimization of Bushing Installation Angle and Bushing Stiffness of Torsion Beam Suspension to Improve the Handing Stability of the Whole Vehicle. *Adv. Mech. Eng.* **2022**, *14*, 16878132221101022. [CrossRef]
29. Adams 2023.4. Adams Car User's Guide. Available online: https://nexus.hexagon.com/documentationcenter/en-US/bundle/Adams_2023.4_Adams_Car_User_Guide/resource/Adams_2023.4_Adams_Car_User_Guide.pdf (accessed on 10 July 2025).
30. Burdzik, R. Impact and Assessment of Suspension Stiffness on Vibration Propagation into Vehicle. *Sensors* **2023**, *23*, 1930. [CrossRef]
31. Von Wysocki, T.; Chahkar, J.; Gauterin, F. Small Changes in Vehicle Suspension Layouts Could Reduce Interior Road Noise. *Vehicles* **2020**, *2*, 18–34. [CrossRef]
32. Mei, Y.; Wang, R.; Ding, R.; Jiang, Y. Classification Evolution, Control Strategy Innovation, and Future Challenges of Vehicle Suspension Systems: A Review. *Actuators* **2025**, *14*, 485. [CrossRef]
33. Wu, T.; Xu, P.; Fu, J.; Su, J. Numerical Modeling and Dynamic and Static Performance Analysis of Hydraulic Mounting. *Actuators* **2025**, *14*, 28. [CrossRef]
34. Žuraulis, V.; Kilikevičius, A. Quarter Car Test Rig for Extended Dynamics Research in Laboratory Conditions. In *Advances in Dynamics of Vehicles on Roads and Tracks*; Klomp, M., Bruzelius, F., Nielsen, J., Hillemyr, A., Eds.; Lecture Notes in Mechanical Engineering; Springer International Publishing: Cham, Switzerland, 2020; pp. 1425–1434, ISBN 978-3-030-38076-2.
35. CORREVIT SFII-P Racing Non-Contact 2-Axis Optical Sensor® for Slip-Free Measurement of Longitudinal and Transversal Dynamics. Available online: https://vre-engineering.com/wp-content/uploads/2020/04/SFII-P-Racing_m-064-p1-e.pdf (accessed on 15 July 2025).
36. Marzbanrad, J.; Soleimani, G.; Mahmoodik, M.; Rabiee, A.H. Development of Fuzzy Anti-Roll Bar Controller for Improving Vehicle Stability. *J. Vibroeng.* **2015**, *17*, 3856–3864.

Disclaimer/Publisher's Note: The statements, opinions and data contained in all publications are solely those of the individual author(s) and contributor(s) and not of MDPI and/or the editor(s). MDPI and/or the editor(s) disclaim responsibility for any injury to people or property resulting from any ideas, methods, instructions or products referred to in the content.